Published in final edited form as:
Nat Med. 2010 March ; 16(3): 286–294. doi:10.1038/nm.2100.

An oncogene-tumor suppressor cascade drives metastatic prostate cancer by coordinately activating Ras and NF-κB

Junxia Min[1,2,3], **Alexander Zaslavsky**[4], **Giuseppe Fedele**[3,5], **Sara K. McLaughlin**[1,2,3], **Elizabeth E. Reczek**[1,2,3], **Thomas De Raedt**[1,2,3], **Isil Guney**[3,5], **David E. Strochlic**[3,5], **E. Laura**[6,7], **Rameen Beroukhim**[2,3,5,7], **Roderick T. Bronson**[3], **Sandra Ryeom**[4], **William C. Hahn**[2,3,5,7], **Massimo Loda**[3,5], and **Karen Cichowski**[1,2,3,7,*]

[1] Genetics Division, Department of Medicine, Boston, MA, 02115, USA

[2] Brigham and Women's Hospital, Boston, MA, 02115, USA

[3] Harvard Medical School, Boston, MA, 02115, USA

[4] Department of Cancer Biology, Abramson Family Cancer Research Institute, University of Pennsylvania School of Medicine, Philadelphia PA 19104

[5] Department of Medical Oncology, Dana-Farber Cancer Institute, Boston, MA 02115

[6] Broad Institute of Harvard and MIT, Cambridge, MA 02142

[7] Ludwig Center at Dana-Farber/Harvard Cancer Center, Boston, MA 02115

Abstract

Metastasis is responsible for the majority of prostate cancer-related deaths; however, little is known about the molecular mechanisms that underlie this process. Here we identify an oncogene-tumor suppressor cascade that promotes prostate cancer initiation and metastasis by coordinately activating Ras and NF-κB. Specifically, we show that loss of the RasGAP gene *DAB2IP* induces metastatic prostate cancer in a murine model. Notably, DAB2IP functions as a signaling scaffold that coordinately regulates Ras and NF-κB through distinct domains to promote tumor initiation and metastasis, respectively. *DAB2IP* is suppressed in human prostate cancer where expression inversely correlates with tumor grade and predicts prognosis. Moreover, we report that epigenetic silencing of *DAB2IP* is a key mechanism by which the polycomb-group protein EZH2 activates Ras, NF-κB, and triggers metastasis. These studies define the mechanism by which two major pathways can be simultaneously activated in metastatic prostate cancer and establish EZH2 as a driver of metastasis.

While early detection has reduced mortality from prostate cancer, there is no curative treatment for advanced disease[1]. Consequently, 1 in 30 men are expected to die from metastatic prostate cancer [1–2]. Nevertheless, our current understanding of the mechanisms that drive progression and metastasis is limited.

Hyperactivation of Ras effector pathways (ERK and AKT) have been proposed to promote prostate cancer progression [3–6]. However while *PTEN*-loss activates AKT, it is unclear how ERK is activated in this tumor-type. *Ras* and *Raf* mutations are present in a subset of tumors

*Correspondence: kcichowski@rics.bwh.harvard.edu; fax (617) 525-4705; phone (617)-525-4722.

Author Contributions

J.M., A.Z., S.K.M., E.E.R., I.G., D.E.S. performed *in vitro* and *in vivo* experiments. G.F., R.T.B, and M.L. analyzed and interpreted the immunohistochemistry and histology experiments. G.F. performed analysis on TMAs. T.D.R performed statistical analysis. L.E.M. and R.B performed Sequenome analysis. S.R., W.C.H, and M.L. provided scientific advice and helpful comments on manuscript. J.M. and K.C conceptualized experiments, prepared figures and drafted manuscript.

from Japanese and Korean patients, but are rare in Caucasian and African-American populations [7–9].

Ras is regulated positively by GEFs (Guanine nucleotide exchange factors) and negatively by GAPs (GTPase-activating proteins) [10–11]. It is unknown whether GEFs play a role in cancer; however, one RasGAP, *NF1*, is a known tumor suppressor [12–15]. Notably, there are 14 human RasGAPs, few of which have been studied in detail. Therefore, we investigated whether other RasGAP genes might also function as tumor suppressors. Here we identify a new tumor and metastasis suppressor within this gene family, define the mechanism(s) by which loss promotes metastatic prostate cancer, and demonstrate that its epigenetic suppression is a key mechanism by which the polycomb-group protein EZH2 triggers metastasis.

Results

DAB2IP suppression drives transformation

To identify tumor suppressors within the RasGAP family we performed a cell-based screen, originally designed to quantify transformation caused by *NF1*-loss [16]. As shown previously, *NF1*-ablation promoted anchorage-independent growth (Fig. 1a). However, suppression of another RasGAP, *DAB2IP*, induced colonies that were larger than *NF1*-deficient clones (Fig. 1b). Importantly, transformation was not generally promoted by the loss of most RasGAPs, including p120RasGAP (Fig. 1a and Supplementary Fig. 1).

We then investigated whether there was evidence linking *DAB2IP*-loss to human cancer. *DAB2IP* expression appears to be selectively suppressed in AML cell lines and in one case was disrupted by a translocation[17]. *DAB2IP* has also been reported to be epigenetically suppressed in advanced lung, breast, and gastrointestinal tumors [18–20]. Intriguingly, *DAB2IP* is among the list of genes repressed by EZH2 in prostate cancer cell lines, a polycomb-group protein thought to promote advanced prostate cancer [21–22]. Nevertheless, the potential tumorigenic consequences of *DAB2IP*-loss have not been investigated.

Given the proposed importance of the Ras/ERK pathway in prostate cancer progression and the lack of a mechanism by which it becomes activated [3–5,14], we explored a role for *DAB2IP*-loss in this process. Primary human prostate epithelial cells (PrECs) are immortalized by introducing hTERT, SV40 Large T and Small t proteins, and androgen receptor (AR) (LHSAR), but these cells are unable to form anchorage-independent colonies[23]. However, the addition of H-Ras^{V12} promotes colony growth and adenocarcinoma when cells are injected into mice[23]. *DAB2IP*-ablation also promoted colony growth, indicating that *DAB2IP*-loss transforms human prostate cells (Fig. 1c). Notably, *DAB2IP*-loss also triggered Ras, ERK and AKT activation (Fig. 1d). These phenotypes were reversed by rescuing cells with a *DAB2IP* cDNA (Fig. 1e, f).

Loss of *DAB2IP* promotes prostate tumor formation and widespread metastasis

When immortalized PrECs were orthotopically injected into mouse prostates, well-circumscribed, benign growths in the prostate developed, as previously described [23]. Lesions exhibited a low proliferative index, significant levels of apoptosis and regressed (9/15 regressed completely) (Fig. 1g and Supplementary Fig. 2a, b). However, animals injected with PrECs expressing oncogenic Ras^{V12} (15/15) or *DAB2IP*-specific shRNAs (15/15), developed prostate adenocarcinomas that expressed cytokeratin 8, PSA, and little p63, similar to high-grade human tumors (Fig. 1g, h). Ras^{V12} and *DAB2IP*-deficient tumors were highly proliferative, exhibited little apoptosis, grew with similar kinetics and to a similar maximum size (Fig. 1g, i, j and Supplementary Fig. 2b,c). Animals injected with DAB2IP-reconstituted cells were similar to controls: most lesions regressed in 45 days and or were small (Fig. 1g, Supplementary Fig. 2c).

However, whereas H-Ras^{V12}-driven tumors remained non-invasive and never disseminated, all *DAB2IP*-deficient tumors were invasive and metastatic (Fig. 2, Supplementary Fig. 2d). Tumors invaded the hip, lumbar muscle, and bladder (Fig. 2b)[24]. Metastases were observed starting at 45 days in liver, proximal and distal lymph nodes, seminal vesicles, testes, and vas deferens (Fig. 2c and Supplementary Fig. 2d). Metastases were derived from PrECs, as confirmed by LgT immunostaining and sequenome-based SNP genotyping (Fig. 2c, d and Supplementary Fig. 3a), and were never observed from cells rescued with *DAB2IP*. Tumor cells could be readily detected throughout lymphatic and blood vessels, implicating both vessel systems in metastasis (Fig. 2d). Animals also developed thromboemboli, a life-threatening complication observed in a subset of prostate cancer patients (Supplementary Fig. 3b)[25]. The metastatic potential of these tumors can be best appreciated by xenogen imaging (Fig. 2e). Mice harboring *DAB2IP*-deficient tumors exhibited reduced survival compared to those with Ras^{V12}-expressing tumors (Fig. 2f; $P = 0.03$ Mann-Whitney U test). Thus, *DAB2IP*-suppression promotes prostate tumorigenesis and uniquely triggers metastasis.

RasGAP activity underlies some but not all of DAB2IP's tumor/metastasis suppressor function

Because DAB2IP is a RasGAP we investigated whether aberrant Ras activation was responsible for these phenotypes. We expanded our analysis to include metastatic human prostate cancer cells in which *DAB2IP* is epigenetically silenced (PC-3 cells), to more directly assess the effects of *DAB2IP*-loss in human cancer [21]. PC-3 and *DAB2IP*-deficient PrEC cells were reconstituted with wild-type *DAB2IP* or a GAP-deficient point mutant. Wild-type DAB2IP had subtle effects on the proliferation of these cell lines *in vitro*, indicating that the reintroduction of physiological levels of DAB2IP does not, by itself, induce a growth arrest (Supplementary Fig. 4). DAB2IP proteins were equivalently expressed and recapitulated endogenous levels (Fig. 3a, b, f). Wild-type DAB2IP reduced Ras-GTP, pERK and pAKT levels, whereas the RasGAP mutant (R289L) did not suppress these effectors (Fig. 3b).

Mice injected with PC-3 cells developed metastatic prostate cancer (Fig. 3c–e). Wild-type DAB2IP significantly suppressed tumor development (Fig. 3d, $P = 3 \times 10^{-8}$, Mann-Whitney U test) and metastasis (Fig. 3c, e); however, DAB2IP-R289L was unable to suppress tumor growth, indicating that RasGAP activity is essential for its tumor suppressive function (Fig. 3c, d; $P = 0.71$). Nevertheless, this mutant partially suppressed metastasis: only 3/6 animals developed metastases and fewer were observed (Fig. 3e; $P = 0.0083$). These findings were confirmed using PrECs (Fig. 3f, g) and suggest that other regions of DAB2IP harbor metastasis-suppressing activity.

DAB2IP is a potent regulator of EMT

Interestingly, *DAB2IP*-ablation in PrECs also induced an epithelial to mesenchymal transition (EMT): a dynamic cellular process thought to underlie metastasis by promoting invasion, intravasation, and extravasation [26–28]. EMT was confirmed by demonstrating an increase in the mesenchymal markers vimentin, twist, and fibronectin, and a concomitant reduction in membrane bound E-cadherin (Fig. 3h, Supplementary Fig. 5)[29]. *DAB2IP* suppression also enhanced invasion (Supplementary Fig. 5a). EMT occurred synchronously within 96 hours and was not due to the outgrowth of a specialized subset of cells (Supplementary Fig. 6). In contrast, Ras^{V12} was a much weaker regulator of EMT (Fig. 3h).

EMT was also observed *in vivo*, as demonstrated by vimentin expression, which was observed in cells at the edge of these highly metastatic lesions (Fig. 3i). This expression pattern was observed in every tumor examined ($n = 12$) and the vimentin detected was present in tumor cells, not stroma, as the antibody exclusively recognizes human protein. Similar findings have been described in a metastatic breast cancer model and support the hypothesis that

environmental cues contribute to EMT and metastasis[28,30]. Ras-expressing tumors never exhibited evidence of EMT (Fig. 3i), supporting the hypothesis that distinct effects of *DAB2IP*-loss on EMT underlie metastasis.

DAB2IP loss promotes metastasis via NF-κB

Although Ras can promote EMT, a plethora of signals regulates this transition [27]. Interestingly, in addition to its RasGAP activity, DAB2IP can suppress NF-κB in endothelial cells through a direct interaction with TRAF2, via a region distinct from the RasGAP domain [31]. Notably, NF-κB plays a critical role in EMT and many EMT-associated genes, including twist, are NF-κB targets [32]. NF-κB also promotes tumor progression and metastasis in other model systems [33]. As such, we asked whether *DAB2IP*-loss triggers EMT and metastasis by activating NF-κB.

Ectopic DAB2IP suppresses NF-κB in endothelial cells, but it was unknown whether *DAB2IP*-loss would activate NF-κB in prostate cells. DAB2IP-ablation activated NF-κB (Fig. 4a) and increased expression of transcriptional targets in PrECs (Fig. 4b) [34]. Conversely, DAB2IP reconstitution suppressed NF-κB and target genes in PC-3s (Fig. 4a, c). A point mutant in the period-like domain of DAB2IP that prevents TRAF2 binding (S604A) is defective in suppressing NF-κB activity in endothelial cells [31]. DAB2IP-S604A did not effectively inhibit NF-κB, but still suppressed Ras (Supplementary Fig. 7a, b). This mutant was also defective in suppressing invasion and EMT, suggesting that NF-κB mediates these phenotypes in response to *DAB2IP*-loss (Supplementary Fig. 7). This was confirmed by introducing a dominant-negative IKBα protein, which suppressed NF-κB activity, invasion and EMT in both model systems (Supplementary Fig. 5 and data not shown). However, consistent with the notion that Ras feeds into the NF-κB pathway [35], the DAB2IP double mutant (R289L and S604A) was more defective in suppressing invasion, EMT, and NF-κB, illustrating cooperativity between these two domains/signals (Supplementary Fig. 7).

Notably, the DAB2IP mutant that effectively suppressed Ras but not NF-κB (S604) inhibited primary tumor growth, supporting the conclusion that Ras is important for tumor initiation (Fig. 4e, h; $P = 1.65 \times 10\text{-}7$, Mann-Whitney U). However, while tumors were small, 5/10 mice developed metastases, suggesting that aberrant NF-κB activity promoted dissemination (Fig. 4f–i). Accordingly, dominant-negative IKBα had no effect on primary tumor development (Fig. 4e, g), but significantly suppressed metastasis (Fig. 4f, g; $P = 0.005$). The DAB2IP double mutant (R289L/S604A) did not suppress primary tumor development ($P = 0.48$) or metastasis ($P = 0.31$) (Fig. 4ei).

We conclude that *DAB2IP*-loss induces the activation of Ras and NF-κB in prostate cancer. Ras plays an essential role in primary tumor growth, whereas NF-κB drives metastasis. Interestingly, we found that while Ras^{V12} and *DAB2IP*-loss activated ERK and AKT in prostate tumors, NF-κB was exclusively activated in *DAB2IP*-deficient tumors as demonstrated by the nuclear versus cytoplasmic staining of NF-κB, supporting the conclusion that DAB2IP has distinct effects on NF-κB (Fig 4j and Supplementary Fig. 8a). Accordingly, we also observed an enhanced inflammatory response in *DAB2IP*-deficient tumors (Supplementary Fig. 8b). These observations challenge the concept that Ras and NF-κB exist in a simple linear pathway in this tumor-type.

DAB2IP is an important EZH2 target

These studies identify a signaling cascade that drives metastatic disease and provide a tractable model system to interrogate the involvement of other genes in metastasis. Another gene implicated in metastatic prostate cancer is *EZH2*, which encodes the histone methyltransferase component of the Polycomb-Repressive Complex 2 (PRC2) and regulates epigenetic gene

silencing [36]. *EZH2* is overexpressed in many tumor types and its expression correlates with tumor grade [36]. *EZH2* was also identified as the most differentially up-regulated gene in metastatic prostate cancer[37]; however, EZH2 has never been shown to drive metastasis, thus a causal role for EZH2 in this process remains to be established.

Over 250 PRC2/EZH2 targets have been identified, including *DAB2IP* [22,38–39]. Therefore we asked whether EZH2 could induce metastatic prostate cancer and investigated the potential contribution of *DAB2IP*-silencing in EZH2-driven phenotypes. Notably, ectopic *EZH2* promoted invasive prostate adenocarcinoma and metastasis to proximal and distal lymph nodes, liver, and spleen (Fig. 5a, Supplementary Table 1). Like DAB2IP-deficient tumors, *EZH2*-driven tumors were detected in lymphatic and blood vessels and mice developed thromboemboli (Fig. 5a).

The observation that EZH2-overexpression phenocopied *DAB2IP*-loss suggested that *DAB2IP* might be a key target of EZH2 in metastatic prostate cancer. EZH2 suppressed DAB2IP protein and mRNA expression in PrECs (Fig. 5b, c), as observed in other cell lines [21]. Chromatin immunoprecipitation indicated that EZH2 was bound to the *DAB2IP* promoter, demonstrating a direct transcriptional suppression of *DAB2IP* by EZH2 (Fig. 5d). When EZH2-expressing cells were reconstituted with endogenous levels of DAB2IP, tumor growth was suppressed and in 2/14 cases tumors eventually regressed (Fig. 5e, $P = 4 \times 10^{-12}$). Moreover, while metastases were detected in animals with EZH2-driven tumors within 8–12 weeks, DAB2IP prevented metastasis, even in animals surviving one year (Fig. 5f). Accordingly, animals injected with DAB2IP-expressing cells survived longer than those injected with cells expressing EZH2 alone (Fig. 5g; $P = 2.3 \times 10^{-4}$, Yates correction).

EZH2 also activated Ras, ERK, AKT and NF-κB, whereas DAB2IP reconstitution significantly suppressed activation (Fig. 5h, 5i). Moreover, like *DAB2IP*-deficient tumors, metastatic EZH2-expressing lesions also underwent EMT at the invasive edge, which was prevented by DAB2IP-reconstitution (Fig. 5h). EMT was also observed *in vitro* (Supplementary Fig. 9). Finally, GAP-domain (R289L) and period-like domain (S604A) mutants had the same effects in EZH2-expressing cells as compared to DAB2IP-deficient PrEC and PC-3 cells on Ras signaling (Fig. 5i), primary tumor growth and metastasis (Fig. 5j). Thus EZH2 activates Ras and NF-κB by epigenetically suppressing DAB2IP, providing the molecular mechanism by which an epigenetic regulator activates these two major signaling pathways (Fig. 6a).

DAB2IP is inactivated in human prostate cancer

DAB2IP deletions have not been reported in human tumors; however, these data suggested that epigenetic suppression might represent an important mechanism of *DAB2IP*-loss in human prostate cancer. While *DAB2IP* has been shown to be a target of EZH2 in a few prostate cancer cell lines [21], its expression has not been examined in human tumors. We validated the DAB2IP antibody (Fig. 6b) and performed immunohistochemical analysis on tissue microarrays containing 589 specimens from 117 patients. Normal basal and secretory cells expressed high levels of DAB2IP (Fig. 6c, e). By contrast, the majority of prostatic intraepithelial neoplasias (PIN) and adenocarcinomas exhibited weak or no DAB2IP expression, which was often restricted to stroma (Fig. 6c–f; Kruskal-Wallis test, $P = 1.8 \times 10^{-27}$). The reduction in DAB2IP can be appreciated in sections containing both normal and cancerous tissue (Fig. 6c). Notably, DAB2IP levels inversely correlated with Gleason grade (Fig. 6f; Kruskal-Wallis, $P = 0.001$; see legend). Finally, using 81 patients for which clinical information was available we found that DAB2IP was significantly lower in patients with a poor prognosis, measured by a shorter time to PSA failure (univariate Cox regression analysis: Hazard Ratio = 0.51, 95% Confidence Interval 0.2 –0.9, $P = 0.03$). Taken together these results support a causal role for *DAB2IP*-loss in human prostate cancer progression.

To investigate whether *DAB2IP*-suppression was caused by EZH2-mediated transcriptional silencing, *DAB2IP* and *EZH2* expression were examined using Oncomine data sets [40]. Consistent with immunohistochemical analysis, DAB2IP mRNA levels were lower in prostate cancer compared to normal prostate tissue and decreased with increasing tumor grade (Fig. 6g; Student's *t* test r = 7.181, $P = 2 \times 10^{-7}$). This was confirmed using 3 additional data sets [40–43]. By comparing *DAB2IP* and *EZH2* in individual tumors and metastases, we also found that *DAB2IP* levels inversely correlated with *EZH2* (Fig. 6h: Collectively, these observations demonstrate that EZH2 and DAB2IP exist in a linear pathway that when deregulated promote metastatic prostate cancer.

Discussion

If detected early, prostate cancer is curable; however, there are no effective therapies for metastatic disease. The current treatment for recurrent prostate cancer is surgical or medical castration. However, patients ultimately relapse and develop androgen-independent, metastatic tumors [44]. Therefore there is a significant gap in our understanding of the mechanisms that underlie prostate cancer progression, metastasis, and in the development of effective therapies.

This knowledge deficit is, in part, due to the lack of tractable model systems. Genetically-engineered mouse models have helped define genes involved in tumor initiation and aspects of tumor progression; however, few models develop metastases and in those that do it is unclear which gene(s) drive this transition [45,46]. Thus orthotopic models represent a platform that can be used in a more high-throughput fashion for gene discovery, in particular for metastasis, which requires numerous prerequisite alterations. In this study we identify *DAB2IP* as a regulator of metastatic prostate cancer. To date, no other gene has been shown to play a direct causal role in driving prostate cancer metastasis, underscoring the significance of this finding and the utility of this model.

These studies also provide insight into mechanisms that regulate tumor initiation versus metastasis. Specifically, *DAB2IP*-loss promotes primary tumor growth by activating Ras and drives metastasis through NF-κB, serving as a signaling scaffold to coordinately regulate these two prominent oncogenic pathways (Fig. 6a). While Ras and NF-κB are known to be activated in advanced prostate cancer, the genetic alterations that confer activation are largely unknown [3–6, 47]. These findings reveal a molecular mechanism by which these two pathways can be activated in prostate cancer.

In some settings Ras can promote NF-κB activation via effects on Ral B and the TBK1 kinase [47–48]; however, here we report that Ras is not sufficient to stimulate NF-κB in prostate tumors. While these observations appear contradictory, a mutation in the GAP domain enhances the effects of a mutation in the period-like domain of DAB2IP (on NF-κB activity), consistent with a cooperative role for Ras in this pathway. NF-κB is regulated by the integrated output of many signals, which may be differentially limiting in different tumor types. The data presented here suggest that DAB2IP is a critical guardian of the NF-κB pathway in prostate tissue.

Finally, these studies suggest that epigenetic suppression of *DAB2IP* by EZH2 is an important mechanism of inactivation in human prostate cancer. Interestingly, while EZH2 is highly expressed in advanced and metastatic prostate cancer[37], it has never been shown to induce metastasis, leading to the unresolved question of whether EZH2 upregulation is a marker or driver of metastasis [49]. These studies establish a causal role for EZH2 in driving metastasis and identify *DAB2IP* as a critical target in this process among numerous target genes, although certainly others may contribute. These observations have important therapeutic implications. Because EZH2 is an enzyme, it has been proposed to be a potential therapeutic target [36]. Our data underscore the utility of developing EZH2 inhibitors, as such agents might suppress both

Ras and NF-κB in prostate cancer: proteins which have proven difficult to target directly. These findings also support the intriguing possibility that such inhibitors might affect primary tumors and metastatic lesions.

Methods

Cell culture

E1A/p53DN MEFs and LHSAR cells were established as previously described [16, 23]. PrECs were obtained from Loza and were grown in defined medium PrEGM as described [23]. PC-3 cells were obtained from ATCC and cultured according to the suppliers' instructions.

Plasmids, retroviral and lentiviral infections

Lentiviral pLKO shRNAs recognizing DAB2IP2IP, NF1, and p120RasGAP were obtained from the Broad Institute RNAi consortium. NF1 shRNA #1: sense 5′-CAACAACTTCAATGCAGTCTT -3′, antisense 5′-AAGACTGCATTGAAGTTGTTG-3′; NF1 shRNA #2: sense 5′-TTATAAATAGCCTGGAAAAGG -3′, antisense5′-CCTTTTCCAGGCTATTTATAA. p120RasGAP shRNA #1: 1 sense 5′-GCTGCCTAACTTATCCATCTT -3′, antisense 5′-AAAAAGCTGCCTAACTTATCC -3′; p120RasGAP shRNA #2: sense 5′-CCCTACATGGAAGGTGTCAAT -3′; antisense 5′-TAAAAACCCTACATGGAAGGTG -3′. EZH2 shRNA#1: sense 5′-CGGAAATCTTAAACCAAGAAT -3′, antisense 5′-CAAAAACGGAAATCTTAAAC-3′; shRNA#2: sense 5′-TATTGCCTTCTCACCAGCTGC -3′; antisense 5′-CAAAAATATTGCCTTCTCACC -3′. Knock-down was assessed by Western blot or Q-PCR as noted. Retroviral and lentiviral infections were performed as described [16,23]. Full length DAB2IP cDNA was amplified via RT-PCR, cloned into pLenti4/V5-DEST vector (Invitrogen), and the sequence was verified. The EZH2 cDNA was cloned into pBabe-myc retroviral vector. The PMMP-luc-neo retroviral luciferase construct was used[48].

Soft agar assay

Sof agar assays were performed with MEFs or PrEC cells as previously described [16]. Colony size was analyzed by ImageJ.

NF-κB reporter assays

2×10^4 cells were seeded in triplicate in 24-well plates. After 18 hours, 100ng of pNF-κB-luciferase (BD Bioscience) or pISRE-luciferase (Stratagene) plus 25ng renilla-encoding plasmid (pRL-TK were transfected in triplicate wells using Fugene6 (Roche). Luciferase activity followed by Renilla activity was measured 36 h after transfection using Dual Luciferase Reporter Assay Kit (Promega). All data were normalized as relative luciferase light/Renilla unit.

Chromatin Immunoprecipitation (ChIP) Assay

ChIP assay was performed as described previously [50] by using ChIP Assay Kit (Upstate).

Immunoblotting and Immunofluorescence

A DAB2IP monoclonal antibody was generated against the last 120 C-terminal amino acids WF17.1 (DFCI core facility). Hybridoma supernatant was used at a dilution of 1: 6. NF1 antibody (Santa Cruz, SC-67D), p120RasGAP (Transduction Laboratories); tubulin (Sigma); phospho-ERK(Ser473), phospho AKT, total ERK and total AKT(Cell Signaling Technologies); E-cadherin (Santa Cruz), human vimentin (DakoCytomation, Glostrup, Denmark); and monoclonal EZH2(BD) or polyclonal EZH2 (Invitrogen). Alexa fluor 488 conjugated with mouse or rabbit secondary antibodies (Molecular Probes) were used for

immunofluorescence. Confocal imaging was performed with Zeiss LSM410 confocal microscopy systems.

Quantitative Real-Time PCR

Total RNA was isolated using Trizol (Invitrogen). Probes for specific genes were obtained from Applied Biosystems. Quantitative real-time PCR was performed using iscript (Applied Biosystems). Each reaction was performed in triplicate and values were normalized to GAPDH.

Orthotopic implantation

Athymic male nude mice (nu/nu; 6 weeks old) were obtained from Jackson Laboratory. Animal handling and experimental procedures were approved by the Center for Animal and Comparative Medicine in Harvard Medical School in accordance with the NIH Guild for the Care and Use of Laboratory Animals and the Animal Welfare Act. Orthotopic implantations were carried out as previously described [23]. Briefly, a suspension of cells 5 10^5/10 μL in 50 μl of 1:1 of PBS: matrigel (BD Biosciences) was injected into the prostate.

Immunohistochemistry and Tissue Microarrays

500 cells were counted from 5 different fields and the percentage of Ki67-positive cells/DAPI positive cells was scored. Human prostate tissue samples were collected following IRB approval at the Brigham and Women's Hospital for construction of tissue microarrays (TMA). Gleason Grade was re-assessed on each individual core to ensure accuracy for these small tissue sections. A standard avidin-biotin complex immunohistochemical protocol was used to evaluate DAB2IP protein expression (1:6 overnight at 4°C). TMA slides were scanned using the Automated Imaging System Ariol SL-50 (Applied Imaging) and images were imported into TMAJ, a web-based software for the management of TMA data. Immunostaining was evaluated blinded to clinico-pathological information and scored as negative (0), weak (1), moderate (2) or strong (3). The average value from replicate cores was used for correlation with clinical outcome. Univariate Cox regression analysis was used to assess the ability of DAB2IP to predict time to PSA failure, defined as a PSA level in the serum greater than 0.2 ng/mL following radical prostatectomy.

Statistical analysis

If data were normally distributed we used the Student's *t* test. Otherwise the Mann-Whitney U test was used. All analyses were performed with the SYSTAT 12 software package. Specific tests are noted in the text and legends.

Gene expression analysis

Gene expression data discussed in this study were retrieved from the Oncomine cancer microarray database.

Xenogen imaging

Animals were imaged with an IVIS-100 CCD camera (Xenogen, Alameda, CA). For anatomical localization, a pseudocolor image representing light intensity (Blue, least intense; red, most intense) was generated in LivingImage and superimposed over the gray scale reference image.

Supplementary Material

Refer to Web version on PubMed Central for supplementary material.

Acknowledgments

The PMMP-luc-neo retroviral luciferase construct was generously provided by Andrew L. Kung and M. Chheda. pRL-TK was a gift from J. Boehm. We thank D. Barbie, J. Boehm and R. Chen for NF-κB reagents and G. Evan for helpful discussions. This grant was supported by in part by the Department of Defense (PC074048) and the Ludwig Center at Dana-Farber/Harvard Cancer Center.

References

1. Nelson WG, De Marzo AM, Isaacs WB. Prostate cancer. N Engl J Med 2003;349:366–381. [PubMed: 12878745]
2. Jemal A, et al. Cancer statistics, 2008. CA Cancer J Clin 2008;58:71–96. [PubMed: 18287387]
3. Jeong JH, et al. BRAF activation initiates but does not maintain invasive prostate adenocarcinoma. PLoS ONE 2008;3:e3949. [PubMed: 19079609]
4. Shen MM, Abate-Shen C. Pten inactivation and the emergence of androgen-independent prostate cancer. Cancer Res 2007;67:6535–6538. [PubMed: 17638861]
5. Gioeli D, Mandell JW, Petroni GR, Frierson HF Jr, Weber MJ. Activation of mitogen-activated protein kinase associated with prostate cancer progression. Cancer Res 1999;59:279–284. [PubMed: 9927031]
6. Malik SN, et al. Immunohistochemical demonstration of phospho-Akt in high Gleason grade prostate cancer. Clin Cancer Res 2002;8:1168–1171. [PubMed: 11948129]
7. Carter BS, Epstein JI, Isaacs WB. ras gene mutations in human prostate cancer. Cancer Res 1990;50:6830–6832. [PubMed: 2208148]
8. Gumerlock PH, Poonamallee UR, Meyers FJ, deVere White RW. Activated ras alleles in human carcinoma of the prostate are rare. Cancer Res 1991;51:1632–1637. [PubMed: 1998954]
9. Cho NY, et al. BRAF and KRAS mutations in prostatic adenocarcinoma. Int J Cancer 2006;119:1858–1862. [PubMed: 16721785]
10. Bernards A, Settleman J. GEFs in growth factor signaling. Growth Factors 2007;25:355–361. [PubMed: 18236214]
11. Bernards A, Settleman J. GAPs in growth factor signalling. Growth Factors 2005;23:143–149. [PubMed: 16019436]
12. Riccardi, VM. Neurofibromatosis: phenotype, natural history, and pathogenesis. The Johns Hopkins University Press; Baltimore and London: 1992.
13. Ding L, et al. Somatic mutations affect key pathways in lung adenocarcinoma. Nature 2008;455:1069–1075. [PubMed: 18948947]
14. Comprehensive genomic characterization defines human glioblastoma genes and core pathways. Nature 2008;455:1061–1068. [PubMed: 18772890]
15. McGillicuddy LT, et al. Proteasomal and genetic inactivation of the NF1 tumor suppressor in gliomagenesis. Cancer Cell 2009;16:44–54. [PubMed: 19573811]
16. Johannessen CM, et al. The NF1 tumor suppressor critically regulates TSC2 and mTOR. Proc Natl Acad Sci U S A 2005;102:8573–8578. [PubMed: 15937108]
17. von Bergh AR, et al. Identification of a novel RAS GTPase-activating protein (RASGAP) gene at 9q34 as an MLL fusion partner in a patient with de novo acute myeloid leukemia. Genes Chromosomes Cancer 2004;39:324–334. [PubMed: 14978793]
18. Dote H, et al. Aberrant promoter methylation in human DAB2 interactive protein (hDAB2IP) gene in breast cancer. Clin Cancer Res 2004;10:2082–2089. [PubMed: 15041729]
19. Dote H, et al. Aberrant promoter methylation in human DAB2 interactive protein (hDAB2IP) gene in gastrointestinal tumour. Br J Cancer 2005;92:1117–1125. [PubMed: 15770214]
20. Yano M, et al. Aberrant promoter methylation of human DAB2 interactive protein (hDAB2IP) gene in lung cancers. Int J Cancer 2005;113:59–66. [PubMed: 15386433]
21. Chen H, Tu SW, Hsieh JT. Down-regulation of human DAB2IP gene expression mediated by polycomb Ezh2 complex and histone deacetylase in prostate cancer. J Biol Chem 2005;280:22437–22444. [PubMed: 15817459]
22. Ke XS, et al. Genome-wide profiling of histone h3 lysine 4 and lysine 27 trimethylation reveals an epigenetic signature in prostate carcinogenesis. PLoS ONE 2009;4:e4687. [PubMed: 19262738]

23. Berger R, et al. Androgen-induced differentiation and tumorigenicity of human prostate epithelial cells. Cancer Res 2004;64:8867–8875. [PubMed: 15604246]
24. Arai Y, et al. Radical prostatectomy for clinically localized prostate cancer: local tumor extension and prognosis. Int J Urol 1996;3:373–378. [PubMed: 8886914]
25. Sorensen HT, Mellemkjaer L, Olsen JH, Baron JA. Prognosis of cancers associated with venous thromboembolism. N Engl J Med 2000;343:1846–1850. [PubMed: 11117976]
26. Scheel C, Onder T, Karnoub A, Weinberg RA. Adaptation versus selection: the origins of metastatic behavior. Cancer Res 2007;67:11476–11479. discussion 11479–11480. [PubMed: 18089773]
27. Thiery JP. Epithelial-mesenchymal transitions in tumour progression. Nat Rev Cancer 2002;2:442–454. [PubMed: 12189386]
28. Weinberg, RA. The biology of cancer. New York: Garland Science; 2007.
29. Yang J, et al. Twist, a master regulator of morphogenesis, plays an essential role in tumor metastasis. Cell 2004;117:927–939. [PubMed: 15210113]
30. Joyce JA, Pollard JW. Microenvironmental regulation of metastasis. Nat Rev Cancer 2009;9:239–252. [PubMed: 19279573]
31. Zhang H, et al. AIP1/DAB2IP, a novel member of the Ras-GAP family, transduces TRAF2-induced ASK1-JNK activation. J Biol Chem 2004;279:44955–44965. [PubMed: 15310755]
32. Huber MA, Beug H, Wirth T. Epithelial-mesenchymal transition: NF-kappaB takes center stage. Cell Cycle 2004;3:1477–1480. [PubMed: 15539952]
33. Naugler WE, Karin M. NF-kappaB and cancer-identifying targets and mechanisms. Curr Opin Genet Dev 2008;18:19–26. [PubMed: 18440219]
34. Hayden MS, Ghosh S. Shared principles in NF-kappaB signaling. Cell 2008;132:344–362. [PubMed: 18267068]
35. Mayo MW, et al. Requirement of NF-kappaB activation to suppress p53-independent apoptosis induced by oncogenic Ras. Science 1997;278:1812–1815. [PubMed: 9388187]
36. Simon JA, Lange CA. Roles of the EZH2 histone methyltransferase in cancer epigenetics. Mutat Res 2008;647:21–29. [PubMed: 18723033]
37. Varambally S, et al. The polycomb group protein EZH2 is involved in progression of prostate cancer. Nature 2002;419:624–629. [PubMed: 12374981]
38. Yu J, et al. A polycomb repression signature in metastatic prostate cancer predicts cancer outcome. Cancer Res 2007;67:10657–10663. [PubMed: 18006806]
39. Kondo Y, et al. Gene silencing in cancer by histone H3 lysine 27 trimethylation independent of promoter DNA methylation. Nat Genet 2008;40:741–750. [PubMed: 18488029]
40. Vanaja DK, Cheville JC, Iturria SJ, Young CY. Transcriptional silencing of zinc finger protein 185 identified by expression profiling is associated with prostate cancer progression. Cancer Res 2003;63:3877–3882. [PubMed: 12873976]
41. Lapointe J, et al. Gene expression profiling identifies clinically relevant subtypes of prostate cancer. Proc Natl Acad Sci U S A 2004;101:811–816. [PubMed: 14711987]
42. Tomlins SA, Rubin MA, Chinnaiyan AM. Integrative biology of prostate cancer progression. Annu Rev Pathol 2006;1:243–271. [PubMed: 18039115]
43. Luo JH, et al. Gene expression analysis of prostate cancers. Mol Carcinog 2002;33:25–35. [PubMed: 11807955]
44. Daskivich TJ, Oh WK. Recent progress in hormonal therapy for advanced prostate cancer. Curr Opin Urol 2006;16:173–178. [PubMed: 16679855]
45. Abate-Shen C, Shen MM. Mouse models of prostate carcinogenesis. Trends Genet 2002;18:S1–5. [PubMed: 12047956]
46. Wang S, et al. Prostate-specific deletion of the murine Pten tumor suppressor gene leads to metastatic prostate cancer. Cancer Cell 2003;4:209–221. [PubMed: 14522255]
47. Henry DO, et al. Ral GTPases contribute to regulation of cyclin D1 through activation of NF-kappaB. Mol Cell Biol 2000;20:8084–8092. [PubMed: 11027278]
48. Barbie DA, et al. Systematic RNA interference reveals that oncogenic KRAS-driven cancers require TBK1. Nature 2009;462:108–112. [PubMed: 19847166]

49. Sellers WR, Loda M. The EZH2 polycomb transcriptional repressor--a marker or mover of metastatic prostate cancer? Cancer Cell 2002;2:349–350. [PubMed: 12450788]

50. Chen H, Toyooka S, Gazdar AF, Hsieh JT. Epigenetic regulation of a novel tumor suppressor gene (hDAB2IP) in prostate cancer cell lines. J Biol Chem 2003;278:3121–3130. [PubMed: 12446720]

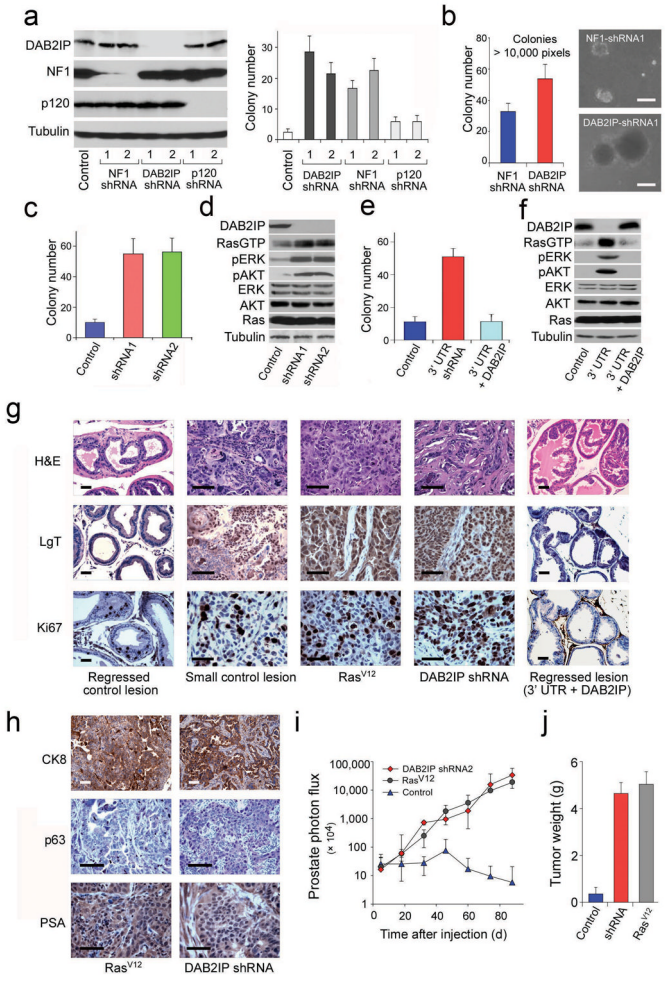

Figure 1. DAB2IP-suppression induces prostate tumor development

(a) Immunoblots showing expression of NF1, DAB2IP or p120RasGAP in E1A and DNp53-expressing MEFs, following lentiviral shRNA expression (left). Colony formation in soft agar (right). Significance determined by a Students t-test. ($P = 3.7 \times 10^{-8}$, $P = 8.6 \times 10^{-9}$). **(b)** Relative size of colonies resulting from loss of *DAB2IP* versus *NF1*. Significance determined by a Students t-test. ($P = .046$) **(c)** Colony formation of immortalized PrEC cells infected with lentiviruses expressing *DAB2IP* shRNA sequences. **(d)** Immunoblots of cells from c to assess DAB2IP knock-down and activation of Ras, ERK and AKT as described in Methods. **(e)** Colony growth induced by *DAB2IP*-suppression using an shRNA directed to the 3′UTR, or rescued with wild-type DAB2IP. **(f)** Immunoblots of cells used in e to assess DAB2IP expression and activation of Ras, ERK and AKT. **(g)** Histological micrographs of tumors resulting from orthotopic injection of PrECs. Top row: hematoxylin and eosin (H&E), middle row: LgT immunohistochemistry, bottom row: Ki67 staining. Note: the first column of images represent prostate tissue from an animal in which a control lesion had regressed. The second column of images is from a small control lesion. The last column is from a prostate in which a "rescued" lesion had regressed. **(h)** Immunohistochemical staining of H-Ras^{V12} and DAB2IP-deficient tumors using antibodies to cytokeratin 8, p63, and PSA. **(i)** Volume of orthotopic tumors over time, calculated by Xenogen imaging (Students t-test (p=.13)). **(j)** Final weight of orthotopic tumors at the time of death (Students t-test (p=.34). All scale bars = 200μM.

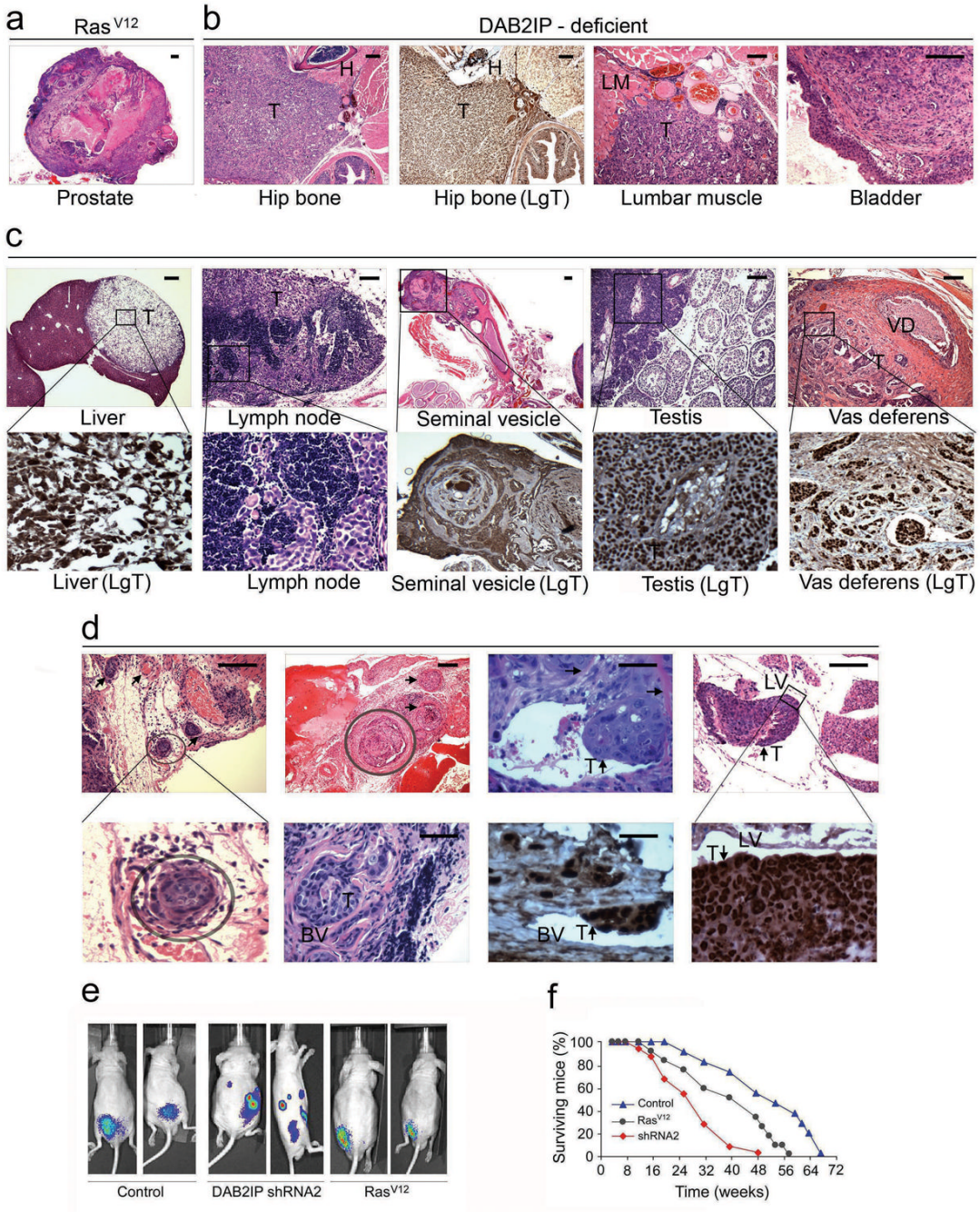

Figure 2. DAB2IP-loss, but not H-Ras^{V12}, promotes invasion and widespread metastasis

(a) Histological micrographs of primary tumors from mice injected with H-Ras^{V12}-expressing PrEC cells. Scale bar = 5mm. **(b)** Histological micrographs of primary tumors from mice injected with *DAB2IP*-deficient PrEC cells. Immunohistochemistry using a LgT antibody is shown in the second panel. Scale bar = 5mm, except lumbar muscle and bladder, scale bar = 1mm. **(c)** Histological micrographs of metastases from mice injected with DAB2IP-deficient PrEC cells. Immunohistochemistry using a LgT antibody on an adjacent section is shown at higher power below each metastasis, with the exception of the lymph node, where on H&E staining is shown. Scale bars (Liver and SV) = 5mM; (LN, testis, VD) = 1nM. **(d)** H&E stained sections of tissues containing tumor cells (T) within blood vessels (BV and arrows) and

lymphatic vessels (LV). When specified by lines higher magnification images are shown. Two panels show LgT staining. Scale bars (panels 1, 2, 4) =1 mM; (panels 3, 5, 6) = 200μM. **(e)** Xenogen images of mice orthotopically injected with luciferase-expressing control, DAB2IP-deficient, or H-Ras^{V12}-expressing cells. **(f)** Survival curves of animals with DAB2IP-deficient versus H-Ras^{V12}-expressing tumors.

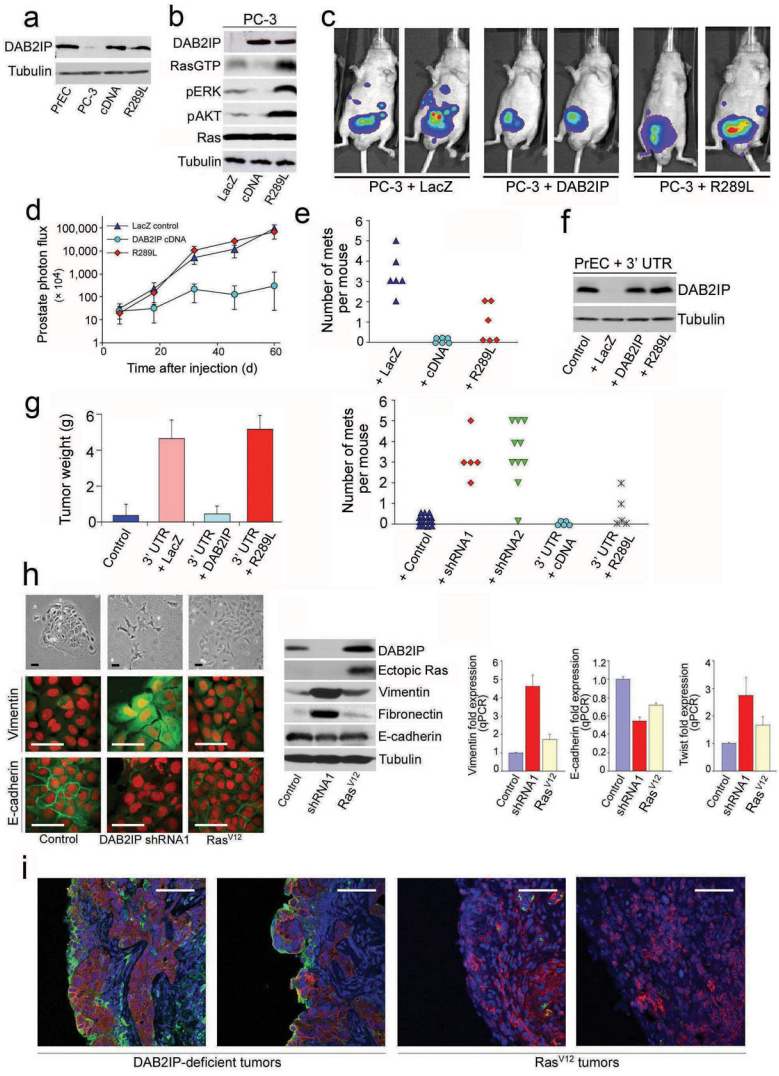

Figure 3. The RasGAP activity of DAB2IP underlies some but not all of its tumor/metastasis suppressor function

(a) Immunoblots comparing DAB2IP expression in PrEC, PC-3, and PC-3 cells expressing wild-type DAB2IP or DAB2IP-R289L. **(b)** Immunoblots assessing effects of DAB2IP and DAB2IP-R289L on Ras, ERK and AKT activation in PC-3s, as described in Methods **(c)** Xenogen images of mice injected with PC-3 cells from a and b. **(d)** Volume of PC-3 derived tumors calculated by Xenogen images. **(e)** Dot plot depicting number of metastases per mouse in animals injected with PC-3 cells expressing wildtype DAB2IP or DAB2IP-R289L. **(f)** DAB2IP immunoblot corresponding to e. **(g)** (Left) Bar graph showing final weight of tumors from PrECs. (Right) A dot plot depicting number of metastases per mouse in animals injected with PrEC cells expressing *DAB2IP* shRNA1 or 2 alone or with the wild-type or DAB2IP-R289L. (Mann-Whitney U; $P = 0.0030$) **(h)** (Top row, left panel) Phase images of immortalized PrEC cells expressing a lentiviral vector control, a DAB2IP-specific shRNA, or an activated Ras allele. (Middle row, left panel) Immunofluorescent staining of the mesenchymal marker vimentin or (Bottom row, left panel) the epithelial marker E-cadherin. (Middle panel) Expression of DAB2IP, ectopic Ras, fibronectin, vimentin, E-cadherin as detected by immunoblot. (Right panel) Real time PCR was performed to quantify vimentin, E-cadherin and twist expression in response to DAB2IP-loss or an activated Ras allele. **(i)** Confocal images

of immunofluorescent staining of vimentin (green) and E-cadherin (red) in DAB2IP-deficient or H-Ras^{V12}-expressing tumors. All scale bars = 100μM.

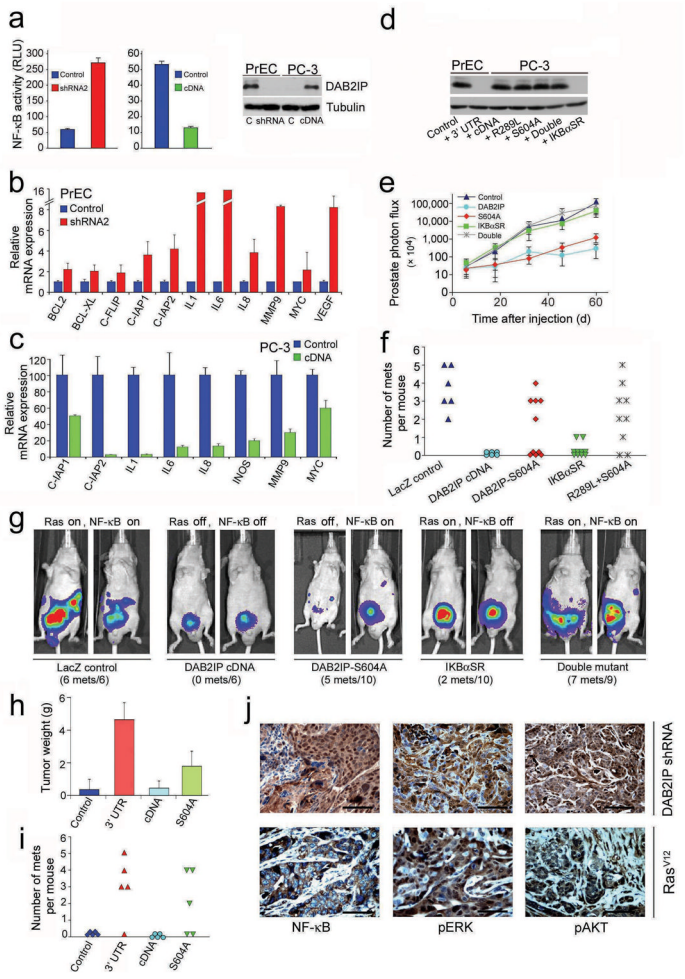

Figure 4. *DAB2IP*-loss promotes tumorigenesis and metastasis via concomitant effects on Ras and NF-κB

(a) (Left) NF-κB activity reported as relative luciferase units (RLU) in response to DAB2IP suppression in PrEC cells. (Middle) NF-κB activity in response to DAB2IP reconstitution in PC-3 cells. (Right) DAB2IP immunoblot. **(b)** Expression of NF-κB targets as determined by Q-PCR in PrEC cells with and without the DAB2IP shRNA in the absence of TNF-α, **(c)** Expression of NF-κB targets as determined by Q-PCR in PC-3 cells with and without the DAB2IP cDNA, in the presence of TNF-α. **(d)** DAB2IP immunoblots of reconstituted PC-3 cells. IκB super-repressor expression shown in Supplementary Fig. 7b. **(e)** Tumor volumes derived from PC-3 cells calculated from xenogen images. **(f)** A dot plot depicting the number of metastases detected in each mouse injected with PC-3 cells. **(g)** Xenogen images of mice injected with PC-3 cells from d-f. The Ras and NF-κB status noted above summarizes the biochemical effects of expressed mutants. The numbers below the images represent the number of animals that develop metastases/the number of animals injected. **(h)** Final weight of tumors derived from control PrEC cells, PrEC cells with the 3′UTR shRNA (3′UTR), 3′UTR cells reconstituted with DAB2IP (cDNA) or the S604A mutant. Expression was determined to be equivalent (not shown). **(i)** A dot plot depicting the number of metastases detected in each mouse injected with the PrEC cells in h. **(j)** Immunohistochemistry using antibodies that recognize NF-κB, pERK, and pAKT in DAB2IP-deficient and H-Ras^{V12}-expressing tumors. Scale bars = 200μM.

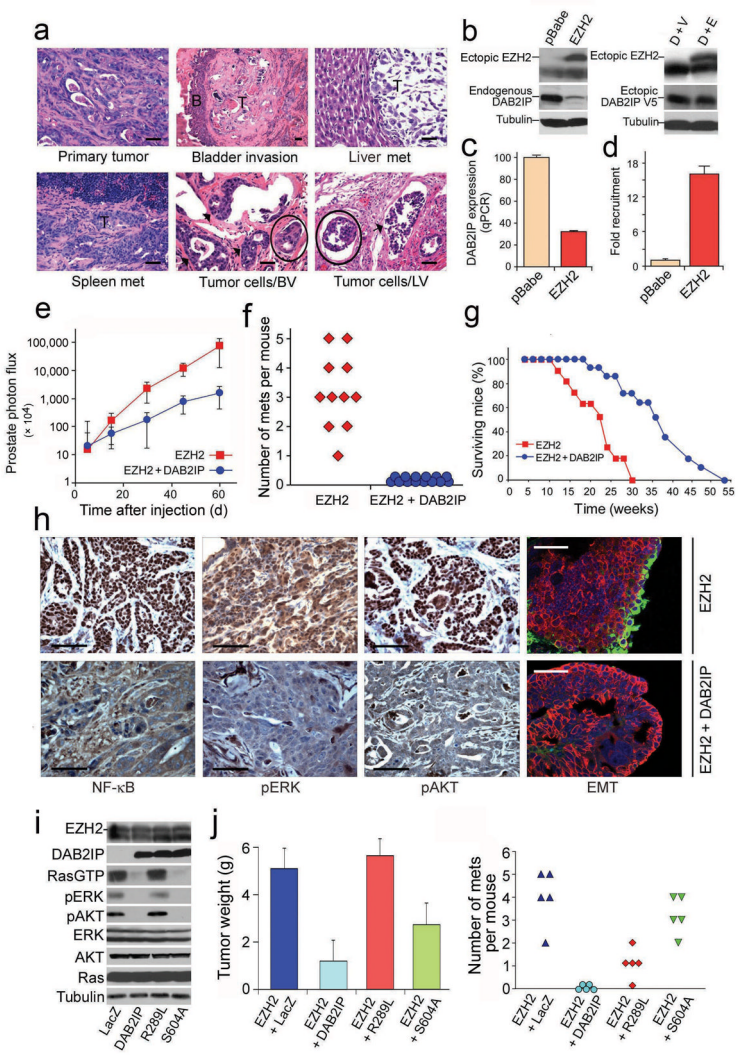

Figure 5. EZH2 promotes tumorigenesis and metastasis via suppression of *DAB2IP*

(a) Histological images of tumors and metastases from orthotopic injection of EZH2-expressing PrEC cells. Tumor cells observed within lymphatic vessels (LV) and blood vessels (BV), circled. Metastasis data for all animals is in Supplementary Table 1. **(b)** (Left) DAB2IP immunoblots of immortalized PrEC cells expressing a vector control or EZH2. The top band is EZH2. (Right) Immunoblots of cells in b reconstituted with ectopic DAB2IP-V5. **(c)** Suppression of endogenous DAB2IP mRNA expression in response to EZH2 as determined by real time PCR. **(d)** Chromatin immunoprecipitation of EZH2 bound to the DAB2IP promoter. **(e)** Tumor volume calculated from xenogen images of animals injected with cells expressing EZH2 or EZH2 and DAB2IP. **(f)** A dot plot depicting the number of metastases detected in each mouse injected with EZH2-expressing or EZH2/DAB2IP-expressing PrEC cells. **(g)** Survival curves of mice injected with orthotopically injected EZH2-expressing or EZH2/DAB2IP-expressing PrEC cells. **(h)** Immunohistochemistry of EZH2-expressing or EZH2/DAB2IP-expressing PrEC derived tumors using p-ERK, p-AKT and NF-κb (p50) antibodies. (Right panels). Confocal immunofluorescence images of of EZH2-expressing or EZH2/DAB2IP-expressing PrEC derived tumors using human vimentin (green) e-cadherin (red) antibodies. **(i)** Immunoblots assessing effects of EZH2 and DAB2IP reconstituion on Ras, ERK and AKT activation in PrEC cells, as described in Methods **(j)** Final weight of tumors

and number of metastases detected in mice injected with cells shown in i. All scale bars = 200μM, except confocal images where scale bars= 100μM.

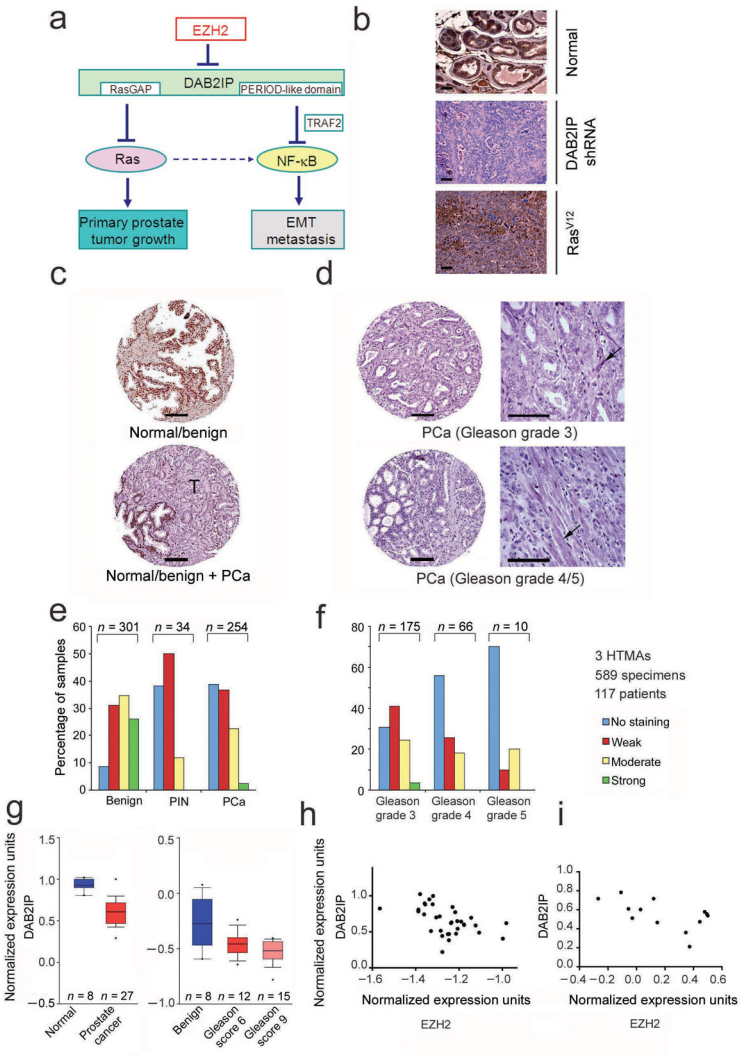

Figure 6. DAB2IP is suppressed in human prostate cancer

(a) Model of how EZH2 regulates DAB2IP, Ras and NF-κB to promote tumor development and metastasis. **(b)** DAB2IP immunohistochemical staining of normal mouse prostate, DAB2IP-deficient PrEC-derived tumors or Ras-driven tumors. **(c)** (Top) Immunohistochemical staining with a DAB2IP antibody in normal human prostate epithelium. (Bottom) Immunohistochemical DAB2IP staining in normal human tissue and adjacent tumor tissue (T) within the same biopsy. **(d)** Immunohistochemical staining with a DAB2IP antibody in human prostate cancer tissues. (Right) High power magnification of images. Arrows depict stromal cells. **(e)** Histogram of DAB2IP protein expression in prostate intraepithelial neoplasia (PIN) and in prostate cancer (PCa) compared to the benign prostate tissue ($P = 1.8 \times 10^{-27}$). **(f)** Histogram comparing DAB2IP expression and Gleason grade (not score), evaluated as the most prevalent pattern on each individual core ($P = 0.001$). Because the tissue sections on the arrays are relatively small, they were assigned a Gleason grade (1–5), rather than a Gleason score (1–10), the latter of which represents the combined total of the two most prevalent grades in an entire tumor. As such, Grade 4 and 5 tumors are high-grade tumors. **(g)** Box plots of DAB2IP mRNA expression data in prostate cancer compared to normal tissue ($P = 2.0 \times 10^{-7}$) and in high grade tumors as opposed to low grade and benign tissue ($P = 0.003$). **(h, i)**

Expression of *DAB2IP* levels versus EZH2 levels in individual tumors and metastatic lesions. All scale bars = 400 μM.